Original Paper

Growth of Large-Diameter $Li_xLa_{(1-x)/3}NbO_3$ Single Crystal by the TSFZ Method Using a Tilting-Mirror FZ Furnace

Most. Umme SALMA[1], Md. Shahajan ALI[2], Yuki MARUYAMA[1,*], Masanori NAGAO[1]
Satoshi WATAUCHI[1], Isao TANAKA[1]

[1]Center for Crystal Science and Technology, University of Yamanashi, 7-32 Miyamae, Kofu, Yamanashi 400-0021
[2]Department of Physics, Pabna University of Science and Technology, Pabna-6600, Bangladesh

Received March 27, 2023; E-mail: myuuki@yamanashi.ac.jp

Large diameter single crystals of $Li_xLa_{(1-x)/3}NbO_3$ with a Li concentration of $x = 0.10$ were grown by using the traveling solvent floating zone (TSFZ) method. A tilting-mirror FZ furnace was the best choice for the high-quality single crystal growth of $Li_xLa_{(1-x)/3}NbO_3$. The required lamp power and convexity were lower for the tilting-mirror FZ furnace than for the conventional FZ furnace. The convexity of the crystal-liquid interface was observed to be low in the case of a $\theta = 10°$ mirror tilt angle. Due to the low lamp power required, little Li evaporated in the tilting-mirror FZ furnace with $\theta = 10°$, which was observed in the quartz tube and EPMA analysis.

Key Words: *Travelling solvent floating zone growth, Growth from melt, Single crystal growth, Oxides, Lithium compounds*

1. Introduction

Solid lithium-ion conductors continue to attract much attention for the development of a next generation solid-state lithium-ion batteries. The reason for this is the increased demand for energy storage from renewable sources and safe batteries with high energy densities, power density and durability. At present, Li-ion batteries have been used in many products, including consumer electronics, electric vehicles (EVs), stationary energy storage systems, cell phones, and portable devices. Although the utilization fields of lithium-ion batteries (LIBs) have been extended from commercial electronics to electric vehicles, LIBs have critical issues because of their highly flammable liquid electrolyte and use of polymer electrolytes, which have a low thermal stability and low flame point. As a result, fire combustion and explosion easily occur because of the long operation time and rough use [1-9]. Additionally, lithium ion cell separators are usually composed of organic solvents and conductive salts that transfer ions. The side reaction occurring between these materials leads to capacity loss and wetting processes during charging and discharging; as a result, extensive lithium dendrite formation is required, which contributes to high costs [10-11].

In contrast, nonflammable, safe and highly reliable solid electrolytes are expected to intensify the energy density, lifetime and safety issues of lithium-ion batteries [12-13]. In all solid-state batteries (ASSBs), a solid electrolyte is used rather than a porous separator soaked with a liquid electrolyte that acts as an insulator and an ionic conductor at a time. The use of a compact solid electrolyte as a physical barrier for lithium dendrite formation on the surface of lithium metal and lithium metal can be used as an anode material. Hence, the volumetric energy density increases by up to 70 % compared to lithium-ion batteries (e.g., graphite used as an anode). Some solid electrolytes with electrochemical stability use a high capacity (sulfur) or high voltage ($LiNi_{0.5}Mn_{1.5}O_4$, LNMO) cathodes, which leads to increased energy densities at the cell level [14-17].

$Li_xLa_{(1-x)/3}NbO_3$ (here after called LLNbO) is a candidate for use in all solid-state batteries as an electrolyte with an ionic conductivity of more than 10^{-4} S·cm^{-1} [18-21]. The ionic conductivity of polycrystalline LLNbO was reported to be $\sigma = 4.7 \times 10^{-5}$ S·cm^{-1} with a lithium concentration of $x = 0.10$. Due to grain boundaries, it is difficult to determine the anisotropic ionic conductivity. On the other hand, the maximum ionic conductivity of LLNbO single crystals was reported to be $\sigma = 3.6 \times 10^{-4}$ S·cm^{-1} with a lithium concentration of $x = 0.08$. The lithium is not homogenously distributed in the grown crystal; furthermore, the lithium concentration increases continuously as crystal growth proceeds. Additionally, the crystal structure of LLNbO varies depending on the lithium concentration [18, 22-23]. The orthorhombic crystal system with $x \leq 0.05$ changes to tetragonal with $x \geq 0.10$ and cubic with $x = 0.25$ with increasing Li fraction x. The crystal structure of LLNbO is a double perovskite in which La^{3+} occupied layers and La^{3+} vacant layers stack alternatively along the c-axis. Hence, the ionic conductivity is anisotropic. The anisotropic ionic conductivity was first reported by using a single crystal of LLNbO, but the crystal was not annealed [19]. The phase diagram of LLNbO, solubility limit and distribution coefficient were reported for growing high-quality crystals. LLNbO shows incongruent melting in $LaNbO_4$ and liquid formation [24]. To grow high-quality single crystals of incongruently melted compounds, such as $Y_3Fe_5O_{12}$ and $La_{2-x}Si_xCuO_4$, the traveling solvent floating zone (TSFZ) is a very good approach. The crucial fact for the TSFZ method is that crystals can be grown at melting points, which potentially reduces vaporization, dislocation densities and nonstoichiometric defect concentrations [25-28]. Recently, for the first time, we have used the TSFZ method to grow homogenous single crystals of LLNbO with a diameter of approximately 6 mm and length of 35 mm. We have also reported the anisotropic ionic conductivity of our LLNbO sample before annealing and after annealing of the grown crystal. The structural changes, lithium concentration-dependent ionic conductivity, activation energy, and lithium concentration distribution of LLNbO were reported [20-21]. However, large-diameter crystals are required for devices and technological applications of all solid-state batteries. However, there are no reports of high-quality, inclusion-free large-diameter single crystals of LLNbO. It is therefore essential and very attractive to grow high-quality single crystals of large-diameter LLNbO.

In the present study, high-quality single crystals of LLNbO with large diameters were grown using a tilting-mirror FZ furnace. Different conditions were imposed to determine the optimum growth conditions for high-quality single crystals. Furthermore, the mirror

tilting effect on the bubble behavior in the molten zone was investigated by quenching the molten zone during TSFZ growth.

2. Experimental

Li_2CO_3 (Rare Metallic Co., Ltd. 99.9%), La_2O_3 (Rare Metallic Co., Ltd. 99.9%) and Nb_2O_5 (Rare Metallic Co., Ltd. 99.9%) have been used as starting raw materials, weighed to achieved a LLNbO (x = 0.10) stoichiometric composition and then mixed. We had observed the highest ionic conductivity in LLNbO single crystals grown using the LLNbO (x = 0.10) feeds in the range of $0.05 \leq x \leq 0.15$ in the previous report [20]. Hence, we focused on Li content of x = 0.10. The mixed powder was calcined at 800 °C for 2 h in air. The calcined powder was ground and calcined again at 1100 °C for 24 h. The calcined powder was again ground and mixed and then formed into a cylindrical shape by rubber pressing under a hydrostatic pressure of 300 MPa. The resultant rod was sintered at 1200 °C for 5 h in air and then used for crystal growth. The feed diameter was approximately 10 mm in each case. Solvents of Li-rich (x = 0.185) and 10 mol% $LaNbO_4$-poor compositions relative to the stoichiometric composition of the LLNbO (x = 0.10) feeds were formed using the same procedure as feed rod formation. LLNbO is an incongruent-melting solid solution in the La_2O_3-Li_2O-Nb_2O_5 system [24]. 10 mol% $LaNbO_4$-poor solvent was effective on suppression of $LaNbO_4$ phase in the LLNbO single crystals since LLNbO melts incongruently to $LaNbO_4$ and a liquid [20]. In addition, Li-rich solvent (x = 0.185) was effective on increase of Li concentration for crystal growth of LLNbO (x = 0.10) since the distribution coefficient of Li into LLNbO solid solution was 0.54 and lower than unity [20, 24].

An optical floating zone furnace (Crystal Systems Inc., Japan; model FZ-T-4000-H) and an image furnace with tilted mirrors (Crystal System Inc., model TLFZ-4000-H-VPO) with four 300 W halogen lamps used as heat sources were used to grow single crystals. Fig.1 shows schematic illustration of conventional and tilting-mirror FZ furnaces. In conventional FZ furnace, the layout of the mirror and heating lamps is in the same horizontal plane. On the other hand, the tilting-mirror FZ furnace, the mirror and heating lamps are tilted from 0º to 20º by a motor drive control [29]. We had reported that the tilting angle θ of 10º is the best condition with minimum convexity of solid-liquid interface and lower required lamp power for crystal growth of $LiCoO_2$ [30]. Hence crystals growth of LLNbO was carried out at 0º and 10° to clarify the tilting angle effects as compared with conventional FZ furnace. The crystal growth conditions were as follows: the growth rate was 5 mm/h in an Ar atmosphere (200 mL/min), the feed and seed rotation rates with opposite directions were 10 rpm and 30 rpm, respectively. A fragment of the grown crystals was used as the seed orientated along [100]. LLNbO single crystals along [100] are considerably useful for electrochemical measurements and battery applications since the maximum ionic conductivity of this materials was found to be along [100] direction [20-21]. The grown crystals were then annealed with an oxygen atmosphere introduced with a 50 mL/min flow at 1000 °C for 24 h.

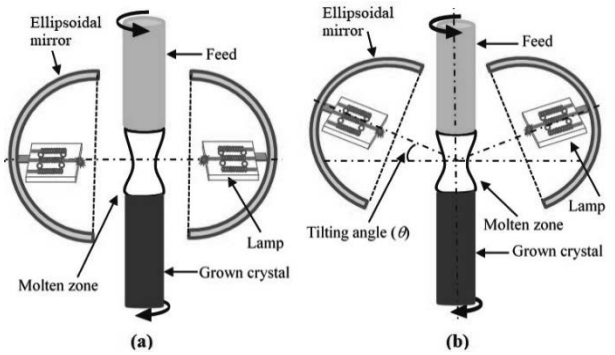


Fig.1 Schematic illustration of (a) conventional FZ furnace and (b) tilting-mirror FZ furnace.

The crystal structure of the grown crystals was identified by X-ray diffraction method (XRD, Bruker Discover D8 with a 2D detector). XRD measurements were performed on cross-sections perpendicular to the growth direction of the O_2-annealed crystals without powdering.

The quenched molten zone and annealed LLNbO single crystals were characterized by compositional analysis. Compositional analysis of the two-dimensional X-ray distribution and quantitative analysis were carried out using an electron probe micro analyzer (EPMA, JEOL Ltd.; model JXA-8200). The O_2-annealed crystals were cut perpendicular to the growth direction and polished with a 1 μm diamond dispersion. The characteristic X-ray intensities of La and Nb were measured by scanning the crystal surface two-dimensionally. Additionally, the concentrations of La and Nb were determined by quantitative analysis using $LaNbO_4$ as a standard sample. The Li concentration x was estimated from the analyzed values of the La and Nb concentrations according to the formula $Li_xLa_{(1-x)/3}NbO_3$.

3. Results and Discussion

First, to grow high-quality single crystals, the optimization conditions for solvent were determined using different amounts of Li-rich and $LaNbO_4$-poor compositions. It was reported that crack and inclusion-free single crystals of LLNbO with 6 mm in diameter were grown using as a solvent of Li-rich (x = 0.185) and 10 mol% $LaNbO_4$-poor compositions relative to the stoichiometric composition of the feed rods [20]. Then, large-diameter crystals were grown using 1.2 g of solvent. First, the conventional FZ furnace was used to grow large-diameter crystals, but crack-free crystals were not found. Some small bubbles were induced, and large bubbles formed together as shown in Fig.2. When the bubbles disappeared, the upper shaft was quickly moved down manually; otherwise, the melt dropped very easily. As a result, the crystal surface became rough, and cracks formed inside the grown crystal. The origin of bubble formation may be due to excess oxygen by reduction of Nb^{5+} in LLNbO feeds at a high temperature and air remaining in the porous feeds. Sintering at high temperatures generally improves the sintering density, but enhanced Li evaporation from the feeds for LLNbO. We had already reported that the growth atmosphere for Ar flow was strongly effective on reduction of bubble formation in the molten zone during TSFZ growth of LLNbO single crystals with 6 mm in diameter [20]. In this study on growth of large-diameter LLNbO single crystals, the bubble behavior in the molten zone was significantly influence on stability of the molten zone during TSFZ growth using the conventional FZ furnace even though under the optimum growth conditions in ref. 20. Therefore, to overcome this problem, we tried to change the heating situation and the solid-liquid interface shape by using a tilting-mirror FZ furnace in order to remove bubbles from the molten zone. For growth using the tilting-mirror FZ furnace at the tilting angle of θ = 0°, some bubbles were observed, but the bubbles were comparatively small. For growth at the tilting angle of θ = 10°, bubble formation was also observed in the molten zone. However, the bubbles were removed easily from the molten zone during growth, and the molten zone was found to be stable.

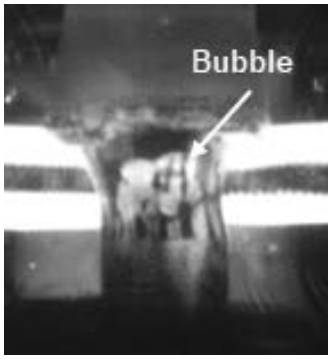


Fig.2 Molten zone of the conventional FZ furnace.

The solid-liquid interface and bubble behavior of the samples in which the molten zone under three different conditions was quenched were measured by EPMA. Fig.3 shows the EPMA analysis of the La concentration distributions. It is clear from all three figures that some bubbles were induced during crystal growth. In the case of the conventional FZ furnace, the bubble size is very large, and if the bubble disappears, it is very easy to melt drop [Fig.3(a)]. For the tilting-mirror FZ furnace with θ = 0°, several small bubbles were observed in the molten zone, as shown in Fig.3(b). On the other hand, Fig.3(c) shows very small bubbles, and there is no effect on crystal growth due to convex interface on the feed side. The convexity of the molten zone is very important for growing high-quality single crystals. Table 1 shows the convexity and required lamp power of the molten zone in different furnaces. The convexity is defined as *h/r*, where *h* is the height from the flat position toward the molten zone in the crystal or feed side, and *r* is the radius of the crystal or feed. Positive and negative values of convexity *h/r* indicate convex and concave interface shapes, respectively. The measured convexity on the crystal side is 0.26, 0.22, and 0.22 for the conventional FZ furnace and tilting-mirror FZ furnace with θ = 0° and θ = 10°, respectively. The interface of the feed side for the conventional FZ furnace shows a concave shape with a convexity of -0.10. The concave interface on the feed side tends to leave bubbles in the center of the melting zone, making it difficult for the bubbles to remove from the molten zone. On the other hands, the interface for the tilting-mirror FZ furnace shows a convex shape with a convexity of 0.10 and 0.16 for θ = 0° and θ = 10°, respectively. The large convexity of the feed side is effective in removing bubbles from the molten zone. Therefore, the tilting-mirror FZ furnace with θ = 10° is effective on the stability of the molten zone during crystal growth due to the large convexity interface on the feed side.

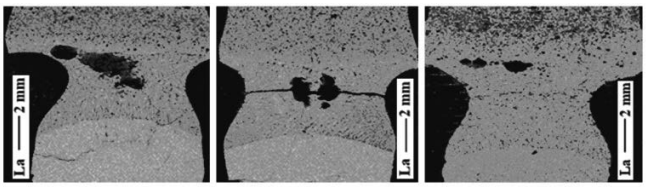


Fig.3 EPMA analysis of quenched samples in the (a) FZ furnace and (b) tilting-mirror FZ furnace with θ = 0° and (c) tilting-mirror FZ furnace with θ = 10°.

Table I Convexity and required lamp power of the quenched molten zone in different furnaces

Condition	FZ furnace	Tilting-mirror FZ furnace	
		(θ = 0°)	(θ = 10°)
Convexity crystal side (*h/r*)	0.26	0.22	0.22
Convexity feed side (*h/r*)	-0.10	0.10	0.16
Lamp power % (4 × 300 W = 1.2 kW)	74.5 (0.67 kW)	66.4 (0.53 kW)	66.0 (0.52 kW)

Lamp power is another important parameter used to reduce evaporation, which is very effective. We used the same lamp power in all cases. We find that the required lamp power is 0.67 kW, 0.53 kW and 0.52 kW for the conventional FZ furnace and tilting-mirror FZ furnace with θ = 0° and θ = 10°, respectively. It is clear that the required lamp power is lower for the tilted mirror FZ furnace than for the conventional FZ furnace. Therefore, a tilting-mirror FZ furnace is effective in suppressing Li evaporation from the molten zone during crystal growth.

During crystal growth, a set of complex physical and chemical processes occur, such as heat transfer, mass transfer in the melt and crystal, impurity processes and impurity redistribution during crystallization, capillary phenomena and evaporation from the melt. Among these conditions, the most crucial condition for growing high-quality single crystals is the temperature gradient in the liquid and solid phases. Temperature gradients are defined by the intensity of the heat sink, chemical composition, release of crystallization heat, heat input to the liquid metal and convective flows in the melt [31]. In particular, the stability of crystallization and quality of the single crystal growth process are mainly affected by the temperature field in the thermal zone. Fig.4 shows the temperature gradient curves obtained for both furnaces. The temperature gradient of the furnaces was observed using 300 W× 4 lamp power and a 40 mm length. The temperature measurement was carried out at the center in an alumina tube with a thermocouple. The temperature gradient is almost the same for both furnaces; however, in the tilting-mirror FZ furnace, the temperature is higher than that in the conventional FZ furnace with the same conditions at the center position. The temperature gradient at the lower portion is 29 °C/mm, which is the same for both furnaces. However, in the upper portion, the temperature gradients in the conventional FZ furnace and the tilting-mirror FZ furnace differ slightly. The temperature gradient in the tilting-mirror FZ furnace is 13 °C/mm, whereas that in the conventional FZ furnace is 17 °C/mm. This indicates that the feed rod in the tilting-mirror FZ furnace is heated to a higher temperature than that in the conventional FZ furnace. The higher heating treatment of the feed enhances the solubility of the feed into the solvent, and increases the convexity in the feed-melt interface as shown in Fig.3(c). As the result, the molten zone was stabilized as compared with the FZ furnace.

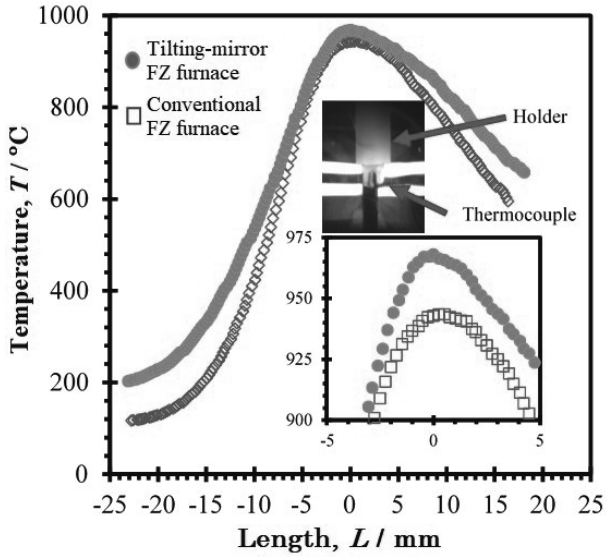


Fig.4 Vertical temperature distribution obtained for the conventional FZ furnace and tilting-mirror FZ furnace.

Fig.5 shows the as-grown crystals and crystals annealed in an oxygen atmosphere. The typical size of the grown crystals was approximately more than 30 mm in length and around 9 mm in diameter. The growth direction was confirmed to be [100] by performing two-dimensional X-ray diffraction in all cases. The grown crystal had a black color and became colorless and transparent by annealing in an O_2 atmosphere at 1000 °C for 24 h. The as-grown crystals have oxygen deficiency and partial reduction of Nb^{5+} to Nb^{4+} by growth in Ar atmosphere. The oxygen deficiency and Nb^{4+} ions in Nb sites were suppressed by annealing in Oxygen atmosphere. For the crystal grown by using the conventional FZ furnace, the crystal shape was not uniform, and the initial and final part was found to be opaque white due to many cracks as shown in Fig.5(a). Cracking in the grown crystals is strongly related with instability of the molten zone due to bubble behavior in the molten zone during crystal growth as mentioned before. The crystal grown with a tilting-mirror FZ

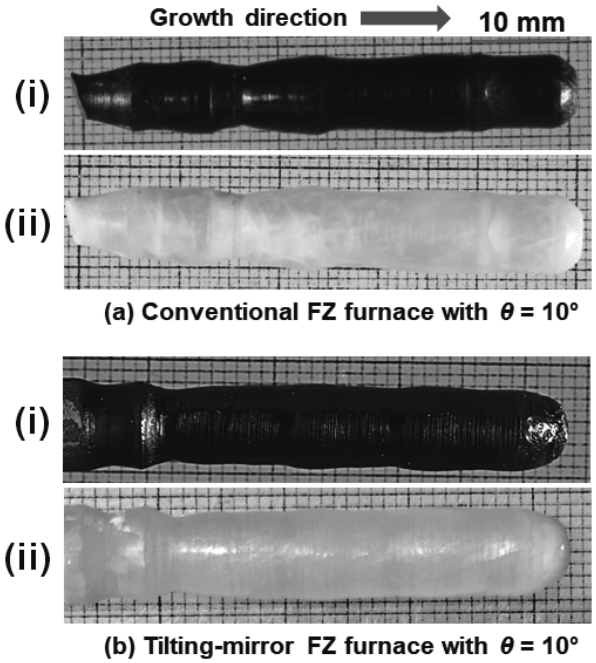


Fig.5 (i) As-grown single crystals and (ii) crystals annealed in oxygen at 1000 ºC for 24 h.

furnace with $\theta = 10°$ has a shinier surface with uniform diameter as shown in Fig. 5 (b). Under the condition of the mirror tilting angle $\theta = 10°$, bubble behavior is no effect on the grown crystal due to a high convexity in the feed-melt interface and a stable molten zone during growth as mentioned before.

Fig.6 shows XRD pattern of the grown crystals. This XRD pattern is consistent with the previous reported data [18]. In particular, the (001) peak, which has about twice the face spacing of (100) and (010), was observed, thereby confirming a double-perovskite structure.

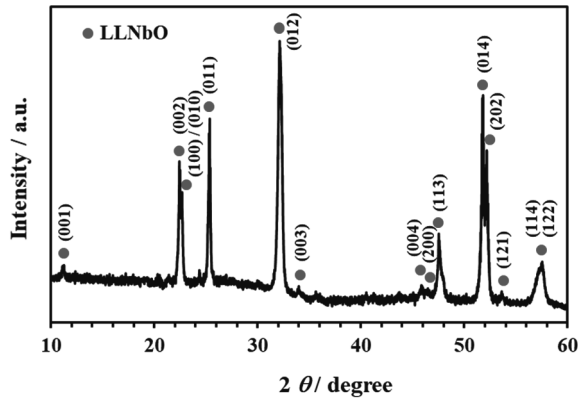


Fig.6 XRD pattern of grown crystals.

The single crystal of LLNbO was confirmed by EPMA analysis. Fig.7 shows the composition distribution in the middle part parallel to the growth direction of the grown crystal. No inclusions were found in the grown crystal. Many black spots in Fig.7 may be due to the voids in grown crystals or dust on the surface of the polished sample. The concentration distribution of Nb and La shows homogeneity according to EPMA analysis. Also, the calculated values of La/Nb atomic ratio and Li concentration x are shown in Table 2. The Li concentration of the crystals obtained using the tilting-mirror FZ furnace is higher than that obtained using the conventional FZ furnace. The Li concentration in the grown crystals is related with the required lamp power and Li evaporation from the molten zone during crystal growth. The Li concentration in the crystals obtained using the tilting-mirror FZ furnace with $\theta = 0°$ and $\theta = 10°$ were almost the same because the required lamp power is the same for both conditions. For crystal growth using the conventional FZ furnace, Li evaporation was enhanced by a higher required lamp power as compared with tilting-mirror FZ furnace since larger amount of lithium compound deposited inside the quartz tube during crystal growth. Finally, we have confirmed that high-quality LLNbO single crystals with a diameter around 9 mm can be grown with good reproducibility using the tilting mirror FZ furnace at the tilting angle $\theta = 10°$.

In our previous research, we have investigated the Li-ion conductivity of LLNbO single crystals with different Li concentrations (0.034 to 0.114) [21]. The ionic conductivity of LLNbO single crystals was found to be maximum at Li concentration ~0.07. Hence, we expect that the large diameter grown single crystals with Li concentration 0.075 will also show high ionic conductivity.

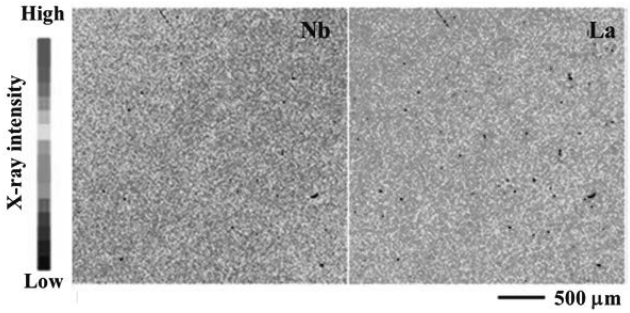


Fig.7 Nb and La X-ray intensity distribution analyzed by EPMA.

Table 2 Atomic concentration of LLNbO grown crystals

	FZ furnace	Tilting-mirror FZ furnace	
		$\theta = 0°$	$\theta = 10°$
La/Nb atomic ratio	0.309±0.001	0.308±0.001	0.308±0.001
Li concentration x	0.071±0.004	0.075±0.002	0.075±0.003

4. Conclusions

Single crystals of LLNbO with large diameters were grown successfully under different conditions using lithium-rich and $LaNbO_4$-poor solvents by the traveling solvent floating zone method. The crystal grown under the 10° tilted mirror conditions was found to be high-quality, homogeneous, and crack- and inclusion-free. The convexity of the tilting-mirror FZ furnace with 10° was found to be minimal, and feed-side convexity was also observed. A high lithium concentration was obtained with tilting-mirror FZ furnace growth. This result indicates that less lithium evaporation occurs during crystal growth in the tilting-mirror FZ furnace than in the conventional FZ furnace. It is concluded that the large-diameter single crystal of LLNbO may be applicable as a solid electrolyte for designing all solid-state batteries. We are planning to use this grown LLNbO crystal in lithium-ion batteries.

Acknowledgement

This work was partly supported by JSPS KAKENHI (grant numbers 21K18906 and 22H04609). M.U.S. was supported by the Graduate Program for Power Energy Professionals, Waseda University, from the MEXT WISE Program. The authors also

gratefully acknowledge technical support from Ruma Parvin at the Independent University.

References

1) P. Knauth, *Solid State Ionics*, **2009**, *180*, 911.
2) J. Schnell, T. Günther, T. Knoche, C. Vieider, L. Köhler, A. Just, M. Keller, S. Passerini, G. Reinhart, *J. Power Sources*, **2018**, *382*, 160.
3) F. Zheng, M. Kotobuki, S. Song, M. O. Lai, L. Lu, *J. Power Sources*, **2018**, *389*, 198.
4) J. Ma, B. Chen, L. Wang, G. Cui, *J. Power Sources*, **2018**, *392*, 94.
5) J.M. Tarascon, M. Armand, *Nature*, **2001**, *414*, 359.
6) M. Armand, J. M. Tarascon, *Nature*, **2008**, *451*, 652.
7) B. Dunn, H. Kamath, J. M. Tarascon, *Science*, **2011**, *334*, 928.
8) D. Larcher, J. M. Tarascon, *Nature Chem.*, **2015**, *7*, 19.
9) S. Chu, A. Majumdar, *Nature*, **2012**, *488*, 294.
10) C. Hendricks, N. Williard, S. Mathew, M. Pecht, *J. Power Sources*, **2015**, *297*, 113.
11) D. L. Wood, J. Li, C. Daniel, *J. Power Sources*, **2015**, *275*, 234.
12) K. Yoshima, Y. Harada, N. Takami, *J. Power Sources*, **2016**, *302*, 283.
13) F. Mizuno, C. Yada, H. Iba, *Lithium-Ion Batteries (Advances and Applications),* Elsevier, Oxford, **2014**, 273-291.
14) A. Varzi, R. Raccichini, S. Passerini, B. Scrosati, *J. Mater. Chem.*, **2016**, *4*, 17251.
15) J. Janek, W.G. Zeier, *Nat. Energy*, **2016**, *1*, 16141.
16) Y. Kobayashi, et al., *J. Electrochem. Soc.*, **2003**, *150*, A1577.
17) J. Li, C. Ma, M. Chi, C. Liang, N. J. Dudney, *Adv. Energy Mater.*, **2015**, *5*, 1401408.
18) Y. Fujiwara, K. Hoshikawa, K. Kohama, *J. Cryst. Growth*, **2016**, *433*, 48.
19) Y. Fujiwara, T. Taishi, K. Hoshikawa, K. Kohama, H. Iba, *Jap. J. App. Phys.*, **2016**, *55*, 090306.
20) M. S. Ali, N. Sato, I. Fukasawa, Y. Maruyama, M. Nagao, S. Watauchi, I. Tanaka, *Cryst. Growth Des.*, **2019**, *19*, 6291.
21) M. S. Ali, Y. Maruyama, M. Nagao, S. Watauchi, I. Tanaka, *Solid Sate Ionics*, **2020**, *350*, 115330.
22) Y. Kawakami, H. Ikuta, M. Wakihara, *J. Solid State Electrochem.*, **1998**, *2*, 206.
23) S. García-Martín, J.M. Rojo, H. Tsukamoto, E. Morán, M. A. Alario-Franco, *Solid State Ionics*, **1999**, *116*, 11.
24) I. Tanaka, R. Yoshihara, C. Nakazawa, M. Nagao, S. Watauchi, *J. Cryst. Growth*, **2019**, *507*, 251.
25) N. Kamaya, K. Homma, Y. Yamakawa, M. Hirayama, R. Kanno, M. Yonemura, T. Kamiyama, Y. Kato, S. Hama, K. Kawamoto, A. Mitsui, *Nat. Mater.*, **2011**, *10*, 682.
26) S. Komura, I. Shindo, *J. Cryst. Growth*, 1977, *41*, 192.
27) I. Tanaka, H. Kojima, Nature, **1989**, *337*, 21.
28) I. Tanaka, K. Yamane, H. Kojima, *J. Cryst. Growth*, **1989**, *96*, 711.
29) S. Nakamura, A. Maljuk, Y. Maruyama, M. Nagao, S. Watauchi, T. Hayashi, Y. Anzai, Y. Furukawa, C. D. Ling, G. Deng, M. Avdeev, B. Büchner, I. Tanaka, *Cryst. Growth Des.*, **2019**, *19*, 415.
30) R. Parvin, Y. Maruyama, M. Nagao, S. Watauchi, I. Tanaka, *Cryst. Growth Des.*, **2020**, *20*, 3413.
31) I. M. Buckley-Golder, C. J. Hurphreys, *Philosophical Magazine*, **1979**, *39*, 41.